Surfactant Effects on Hydrogen Evolution by Small Molecule Non-Fullerene Acceptor Nanoparticles

Andrew Dolan,[†] Jessica M. de la Perrelle,[†] Emily R. Milsom,[†] Thomas D. Small,[†] Gregory F. Metha,[†] Xun Pan,[‡] Mats R. Andersson,[‡] David M. Huang,[†] and Tak W. Kee*,[†]

[†]*Department of Chemistry, The University of Adelaide, Adelaide, South Australia, 5005, Australia*

[‡]*Flinders Institute for NanoScale Science & Technology, Flinders University, Bedford Park, South Australia, 5042, Australia*

E-mail: tak.kee@adelaide.edu.au

Phone: +61-(0)8-8313-5314

Abstract

Organic donor:acceptor semiconductor nanoparticles (NPs) formed through the miniemulsion method have been shown to be active photocatalysts. Here we report photocatalytic hydrogen (H_2) evolution under sacrificial conditions with Pt as a co-catalyst by NPs comprising only the non-fullerene acceptor Y6, stabilized by either sodium dodecyl sulfate (SDS) or the thiophene-containing surfactant 2-(3-thienyl)ethyloxybutylsulfonate sodium salt (TEBS). Typically, changes in the photocatalytic activity of donor:acceptor NPs are associated with differences in morphology due to the use of surfactants. However, as these NPs are single-component, their photocatalytic activity has a significantly lower dependence on morphology than two-component donor:acceptor NPs. Results from ultrafast transient absorption spectroscopy show a minor difference between the photophysics of the TEBS- and SDS-stabilized Y6 NPs, with free charges present with either surfactant. The similar photophysics suggest that both TEBS- and SDS-stabilized Y6 NPs would be expected to have similar rates of H_2 evolution. However, the results from photocatalysis show that Y6 NPs stabilized by TEBS have a H_2 evolution rate 21 times higher than that of the SDS-stabilized NPs under broadband solar-like illumination (400–900 nm). Transmission electron microscopy images of the Y6 NPs show effective photodeposition of Pt on the surface of the TEBS-stabilized NPs. In contrast, photodeposition of Pt is inhibited when SDS is used. Furthermore, the zeta potential of the NPs is higher in magnitude when SDS is present. Hence, we hypothesize that SDS forms a dense, insulating layer on the NP surface which hinders the photodeposition of Pt and reduces the rate of H_2 evolution. This insulating effect is absent for TEBS-stabilized Y6 NPs, allowing a high rate of H_2 evolution. The TEBS-stabilized Y6 NPs have a H_2 evolution rate higher than most single-component organic photocatalysts, signaling the potential use of the Y-series acceptors for H_2 evolution in Z-scheme photocatalysis.

Introduction

Hydrogen (H_2) as a renewable fuel source is attracting significant attention, with many countries investing in H_2 technology as a means to reach net zero carbon emission targets.[1–3] The current methods of producing H_2 are either non-renewable, in the case of steam methane reforming, or expensive to implement, in the case of photovoltaic (PV) electrolysis.[4,5] These limitations have led to the popularization of H_2 evolution via particulate photocatalysis. Photocatalysis offers significant cost reductions by integrating solar light-to-charge generation with water electrolysis, resulting in an aqueous suspension of photocatalytic nanoparticles (NPs) that absorbs light, generates charges, and drives water splitting in a single particulate system.[6,7] Although NP photocatalysts offer the highest degree of integration of solar light harvesting and H_2 evolution, many photocatalysts are unable to function in the absence of a co-catalyst, which is typically deposited on the NP surface.[7] The dependence on co-catalysts is largely due to the recombination of free electrons and holes in the NP bulk before they can participate in reduction and oxidation reactions. Co-catalysts, which are often noble metals, suppress this charge recombination by offering a surface site for charges to accumulate, providing physical separation between free electrons and holes.[8]

Many of the highest performing photocatalysts currently used for H_2 evolution are comprised of inorganic materials. Most inorganic materials only absorb UV light, limiting their efficiency under solar illumination to $\sim$2 %.[9] Organic materials have the potential to improve on this efficiency limit due to their capacity to absorb and utilize visible light. Recently, organic donor:acceptor NPs have demonstrated high rates of H_2 evolution under visible light illumination.[10–12] Unfortunately, although this extended light absorption increases the number of absorbed photons, it can often lead to the loss of sufficient driving force for either the reduction of H^+ or oxidation of water.[8] All donor:acceptor blends reported so far lack the required electrochemical potentials to achieve oxidation of water. Therefore, a sacrificial electron donor such as ascorbic acid has been used to study H_2 evolution in donor:acceptor NPs (Figure 1a).

A method of increasing visible light absorption while retaining a driving force for water splitting is Z-scheme photocatalysis.[13] Z-scheme photocatalysts use two catalysts, a hydrogen-evolving photocatalyst (HEP) and an oxygen-evolving photocatalyst (OEP), targeting the reduction of H^+ and the oxidation of H_2O, respectively. The two catalysts are coupled physically by a conductive medium that allows electrons to flow from the OEP to the HEP, restoring charge neutrality in both materials. Since organic materials are largely unable to facilitate H_2O oxidation, but have high rates of H_2 evolution, they have been identified as possible HEPs for Z-scheme photocatalysts.[12,14] However, organic photocatalysts generally have a lower efficiency than inorganic photocatalysts.[7,15] Hence, further optimization of organic materials is required if they are to be used in Z-scheme photocatalysts, and it is critical to understand the factors that limit and enhance their photocatalytic activity.

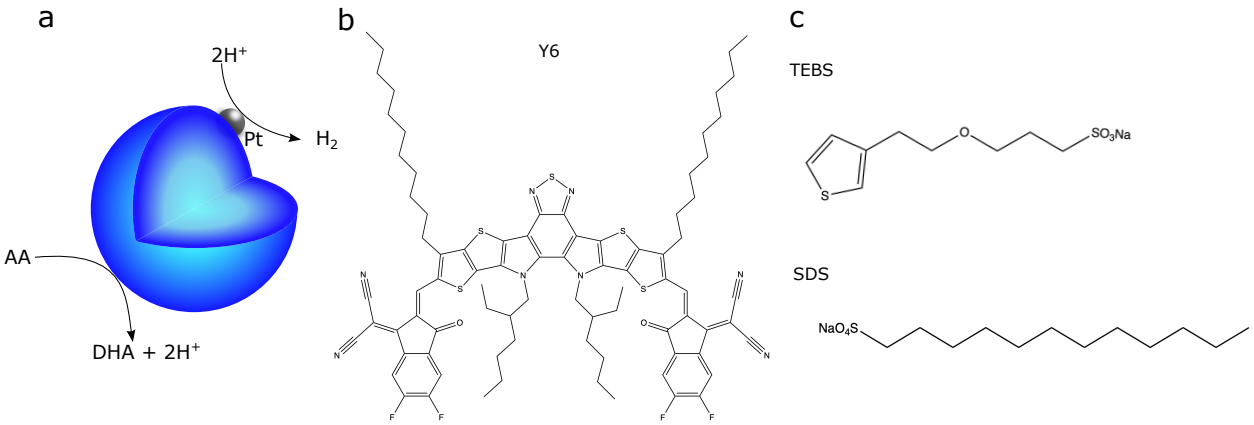

Figure 1: (a) Schematic of H_2 evolution by a single-component NP under sacrificial conditions. H_2 is evolved by reduction of H^+, facilitated by a Pt NP co-catalyst. In the oxidation pathway, sacrificial reagent ascorbic acid (AA) is oxidized to dehydroascorbic acid (DHA), producing H^+. Chemical structures of (b) Y6, and (c) surfactants 2-(3-thienyl)ethyloxybutylsulfonate sodium salt (TEBS) and sodium dodecyl sulfate (SDS).

The formation of organic donor:acceptor blend NPs is often achieved through the miniemulsion method, in which a surfactant is used to stabilize the NP dispersion in an aqueous medium.[16] In some high-performing donor:acceptor systems, changes in performance have been attributed to differences in morphology arising from the use of different surfactants.[11] Previously, studies have shown that the commonly used surfactant SDS typically produces

NPs in which the donor and acceptor adopt a core–shell morphology, in which one component forms a shell around a core of the other component.[17] The use of the relatively new thiophene-containing surfactant TEBS has been shown to produce NPs with an intermixed morphology, in which donor and acceptor domains are small and evenly dispersed throughout the NP.[11,12,18] NPs with intermixed morphologies are expected to have higher photocatalytic activity than those with core–shell morphologies for two reasons. First, for both the oxidation and reduction reactions to occur, surface sites of both the donor and the acceptor must be available to facilitate both reactions. Second, an intermixed morphology provides a greater donor–acceptor interface area, increasing the efficiency of free charge generation. So far, research on organic NP preparation using different surfactants has been focused on the effect that the surfactant has on the morphology of the NP. However, there has been less work on the effect of different surfactants on the surface reactions that are critical to photocatalysis.

This article presents an investigation into how two surfactants affect photocatalytic H_2 evolution in the absence of differences associated with core–shell or intermixed morphologies. We produced NPs comprised of small-molecule organic semiconductor Y6 (Figure 1b) using the miniemulsion method, stabilized by either TEBS or SDS (Figure 1c). The Y6 molecule is part of a class of organic semiconductors known as non-fullerene acceptors (NFAs).[19,20] NFAs have pushed the limits of efficiency in organic PV cells, with Y6 itself demonstrating a unique packing structure and the ability to generate long-lived free charges in donor:Y6 thin films.[21–25] Y6 also has an exceptionally low exciton binding energy ($\leq 0.15\,\mathrm{eV}$[26]), and has been shown to generate free charges even in the absence of an electron donor.[26,27] Additionally, Y6 has a electron affinity of $-4.10\,\mathrm{eV}$ relative to the vacuum potential, appropriate for the reduction of H^+ to H_2 (Figure S1).[28] Hence, Y6 NPs have significant potential for photocatalytic H_2 evolution. Indeed, Y6 NPs formed by the miniemulsion method using TEBS have been shown to evolve H_2 under sacrificial conditions.[12] In itself, this observation is somewhat unusual as high photocatalytic performance from single-component small-

molecule organic NPs is rarely demonstrated.

Here, we found that under sacrificial conditions with a Pt co-catalyst, TEBS-stabilized Y6 NPs evolve H_2 at a rate of $4200 \pm 400\,\mu mol\,h^{-1}\,g^{-1}$. This H_2 evolution rate is higher than most donor–acceptor co-polymer NPs.[7] Interestingly, we also observed that TEBS-stabilized Y6 NPs evolve H_2 at a rate 21 times higher than SDS-stabilized Y6 NPs. To rationalize the difference in rate, we observed by transmission electron microscopy (TEM) that SDS inhibits the photodeposition of the Pt co-catalyst on the NP surface. Additionally, we found that the zeta potential is higher in magnitude in the NPs stabilized with SDS compared to those stabilized with TEBS. This increase in zeta potential magnitude indicate that the surface charge density of the NPs is higher when SDS is used. Hence, we propose that SDS may form a denser layer of surfactant on the NP surface than TEBS, potentially hindering Pt photodeposition. Finally, using ultrafast transient absorption (TA) spectroscopy we confirmed that there is a minor difference in the photophysics of the NPs prepared with the two surfactants; in particular, free charges are formed in both SDS-stabilized and TEBS-stabilized Y6 NPs. Hence, the overall results show that the low H_2 evolution rates of the SDS-stabilized NPs are likely due to SDS forming a dense, insulating layer on the NPs surface, which prevents effective photodeposition of the Pt co-catalyst and hence reduces the H_2 evolution rate. This result indicates that the detrimental effects of SDS in donor:acceptor systems, in addition to the previously noted promotion unfavorable core–shell morphologies, may be due SDS inhibiting the photodeposition of co-catalysts. Furthermore, we demonstrate that the use of TEBS as an alternative surfactant to SDS is beneficial even in single-component NP systems.

Experimental

Materials

Y6 (also known as BTP-4F) was purchased from Ossila and used without further purification. TEBS and SDS were purchased from Solaris and Chem Supply respectively. Chloroform ($CHCl_3$) was purchased through Chem Supply. Water used was purified with an 18 MΩ Millipore Milli-Q reagent water system with a 0.45 µm filter. Photodeposition of platinum was achieved using chloroplatanic acid hexahydrate (K_2PtCl_6), purchased from Sigma Aldrich (CAS no. 97-13-7), with sacrificial reagent *L*-ascorbic acid (99%) purchased from Chem Supply.

Nanoparticle Preparation

The organic material Y6 (3 mg) was added to 1.0 mL of $CHCl_3$. An aqueous surfactant solution was prepared by adding desired surfactant (33 mg) to 2.4 mL of water. Both solutions were dissolved by stirring (500 rpm) at a constant temperature of 30 °C for approximately 20 h. The aqueous and organic solutions were then combined to form a macro-emulsion through stirring (1200 rpm) for 1 h at 60 °C. A miniemulsion was formed through ultrasonication of the mixture with amplitude set to 30 % for three 1-minute intervals, cooling the solution in an ice bath for ∼20 s between each interval. All miniemulsions were produced using a Vibra-Cell ultrasonic processor VCX 750 with stepped probe (tip size 1/8″). After ultrasonication, the miniemulsions were immediately transferred to a heating block where $CHCl_3$ was removed through evaporation at 60 °C for 3 h, stirring at 1200 rpm. An addition of 1 mL of water after 1.5 h countered any excess concentration of the NPs during the solvent removal. Excess surfactant was removed through centrifugal dialysis, first for 7 min at 4000 rpm, and then decreased to 6 min at 4000 rpm. The number of 6-minute dialysis cycles varied with surfactant; TEBS samples required only a single 6-minute cycle, while SDS samples required six 6-minute cycles.

Dynamic Light Scattering and Zeta Potential

All dynamic light scattering (DLS) and zeta potential measurements were conducted using a Malvern Instruments ZetaSizer Nano S, using a wavelength of 633 nm at a power output of 10 mW, with backscattering angle of 173°. For DLS, samples were diluted to 20 ppm and loaded into disposable plastic cuvettes, with a path length of 1 cm. For zeta potential measurements, 20 ppm NP suspensions were loaded in disposable folded capillary cells (DTS1070), with cells having been flushed prior with methanol followed by Milli-Q water to facilitate wetting.

Steady-State Spectroscopy

Steady-state UV-visible absorption spectra were obtained using a Cary 1E UV-visible spectrophotometer in a 2-mm path length quartz cuvette (Starna cells, 21-Q-2).

Transmission Electron Microscopy

An FEI Tecnai G2 Spirit with an accelerating voltage of 120 kV was used to collect TEM images. To prepare samples for TEM, a small drop of NP suspension (30 ppm) was deposited onto a continuous carbon/formvar grid and allowed to evaporate to dryness (∼1 h). The grids were cleaned prior to deposition with a GATAN Solarus 950 Advanced Plasma Cleaner (oxygen/hydrogen plasma, 10 W) for 15 s.

Photodeposition of Platinum Co-Catalyst and Photocatalytic H_2 Evolution

Photocatalytic evolution of H_2 by Y6 NPs was achieved using the sacrificial electron donor ascorbic acid, and platinum (2 wt%) as a co-catalyst. A suspension of NPs (0.225 mg) in water (3 mL) with sacrificial reagent ascorbic acid (0.2 M) and K_2PtCl_6 solution (8.6 µL, 1.33 mg/mL) was added to a liquid batch reactor (13 mL volume, 1.77 cm^2 top-down illumi-

nation area, diagram shown in Supporting Information, Figure S4). Overhead illumination of sample by a Xe arc lamp (300 W, Stryker X6000, spectrum in Figure S6) at solar intensity (100 mW/cm^2), facilitated in-situ photodeposition of Pt and H_2 evolution. Prior to each reaction, air was evacuated and replaced with argon gas at atmospheric pressure. The reaction was stirred continuously, and 500 µL was sampled hourly with 400 µL externally injected into a gas chromatograph (Agilent 7890B GC, Argon carrier gas).

Quantum Efficiency Measurements

The external quantum efficiency (EQE) was determined through

$$\mathrm{EQE}\,(\%) = \frac{2\,n_{\mathrm{H_2}}}{I} \times 100\% \tag{1}$$

where $n_{\mathrm{H_2}}$ is the number of moles of H_2 produced per hour and I is the number of incident photons over a 1-hour period, with the factor of 2 accounting for the number of electrons required to produce one molecule of H_2. Note that when the sample absorbs the majority of the incident light, the EQE is equivalent to the apparent quantum yield (AQY).[29] Aqueous NP suspension, K_2PtCl_6 solution, and ascorbic acid were added to the liquid batch reactor as previously described. Overhead illumination of the sample by a Xe arc lamp (300 W, Stryker X6000) at solar intensity (100 mW/cm^2), facilitated in-situ photodeposition of Pt for 3 h. After 3 h, the reactor was purged and the internal gas was replaced with argon at atmospheric pressure. The internal gas was then sampled to determine the level of residual H_2. To calculate the EQE, the hydrogen production was measured for a further 4 h under illumination by 780 nm light generated by a Thorlabs LED (M780L3) at 6.1 mW/cm^2. Incident photon calculations are given in the Supporting Information, Section S4.

Transient Absorption Spectroscopy

Time-resolved absorption experiments were performed using a home-built TA spectrometer. Pump pulses at 808 nm with a ∼230 fs instrument response function were generated using an optical parametric amplifier pumped with a 1030 nm pulsed laser with a repetition rate of 5 kHz (Light Conversion, Pharos). The probe was generated by focusing the 1030 nm output onto a 12.5 mm sapphire. The pump and probe were polarised at the magic angle (54.7°) relative to each other. Spot sizes (full-width-at-half-maximum) were 93 ± 9 µm for the probe and 510 ± 20 µm for the pump. The signal was detected with a spectrograph (Newport, 77400) and camera (Andor, Zyla sCMOS). TA measurements were taken with samples at 30 ppm in 2-mm path-length quartz cuvettes (Starna Cells, 21-Q-2) and samples were stirred continuously during the experiment. Minimal photo-degradation was observed for all samples. Savitzky-Golay filtering[30] was applied to smooth the data, with a polynomial order of two.

To prepare platinized Y6 NP for TA, TEBS-stabilized Y6 NP (0.315 mg in 4.2 mL) and aqueous K_2PtCl_6 solution (12 µL, 1.33 mg/mL) were added to the liquid batch reactor and platinized for 3 h under white-light illumination as described in the photocatalysis methods. To prepared platinized NP with ascorbic acid, ascorbic acid (0.2 M) was also added to the liquid batch reactor before the platinization. After platinization, the NPs were diluted to 30 ppm for TA experiments. In the Supporting Information, it is shown that the presence or absence of ascorbic acid during the 3 h illumination under white light had minimal impact on the platinization (Figure S3) and the subsequent H_2 evolution rate under 780 nm light (Figure S5).

Results and Discussion

Nanoparticle Characterization

The UV–visible absorption spectra of Y6 NPs prepared with either SDS or TEBS (Figure 2) show broad absorption from 600–850 nm, with three peaks. In chloroform solution, time-dependent density functional theory has been used to assign the lowest-energy peak (∼815 nm) and a shoulder at ∼730 nm to the vibronic progression of the $S_0 \rightarrow S_1$ transition and the 670 nm peak to the $S_0 \rightarrow S_2$ transition.[31,32] In these NPs, the three peaks appear approximately in the same location as the corresponding peaks in Y6 films,[31] with a significant change in relative peak heights which results in a very broad, near-uniform absorption between 650 nm and 820 nm. The choice of surfactant has a negligible effect on the absorbance of the NPs, with the only difference being a slightly lower amplitude of the ∼820 nm peak for the SDS-stabilized NPs. The broad absorption profile has been observed previously in Y6 NPs prepared by re-precipitation.[33] In comparison, the spectra in Figure 2 have a lower relative amplitude of the 820 nm peak, likely due to the difference in preparation method.

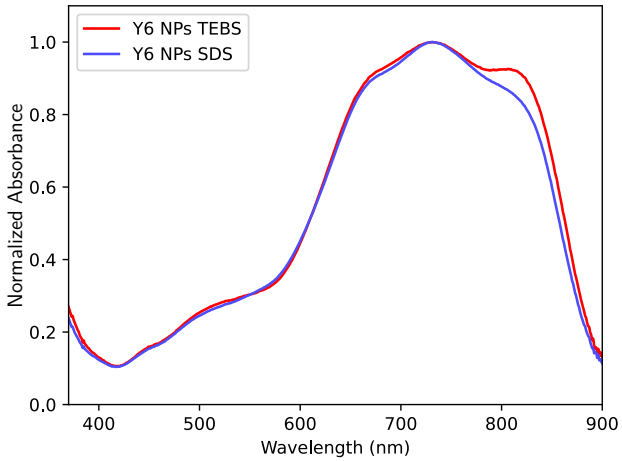

Figure 2: Normalized UV–visible absorption of Y6 NPs stabilized with SDS or TEBS.

DLS was used to measure the *Z*-average diameter and polydispersity index (PDI) of the Y6 NPs. The NPs had a *Z*-average diameter of 78.3 ± 0.5 nm and 48.5 ± 0.3 nm for TEBS- and SDS-stabilized NPs, respectively. Full intensity distributions can be found in

the Supporting Information, Figure S2. The NPs prepared with SDS were somewhat more polydisperse than those prepared with TEBS.

Table 1: Z-average diameter (D_Z) and PDI of Y6 NPs.

Sample	D_Z **(nm)**	**PDI**
Y6 NPs TEBS	78.3 ± 0.5	0.235
Y6 NPs SDS	48.5 ± 0.3	0.302

Photocatalytic Hydrogen Evolution

Recent developments in photocatalytic H_2 evolution by organic donor:acceptor blends have involved polymeric donors paired with NFAs. Y6 is a small-molecule NFA which has been shown to achieve high efficiency in organic PV cells,[28] and has also demonstrated the ability to evolve H_2 in the presence of sacrificial electron donor ascorbic acid.[12] Work by Kosco et al. demonstrated H_2 evolution from Y6 NPs formed through the miniemulsion method with TEBS as a stabilizing surfactant.[12] Here we compare Y6 NPs prepared with both TEBS and SDS surfactants and find a 21-fold difference in the rate of H_2 evolution.

Figure 3a shows the H_2 evolved over time by Y6 NPs stabilized with TEBS and SDS, with TEBS-stabilized Y6 NPs having a H_2 evolution rate of 4200 ± 400 µmol h^{-1} g^{-1}. This rate is ∼1.5 times lower than the rate reported by Kosco et al. for TEBS-stabilized Y6 NPs. A lower rate is expected here as a lower Pt loading was used in this work (2 % compared to 10 %).[12] NPs stabilized with TEBS achieved an EQE of 0.054 ± 0.001 % under 780 nm illumination (Figure 3b–c). In contrast to TEBS-stabilized Y6 NPs, Y6 NPs stabilized with SDS had a significantly lower H_2 evolution rate of 110 ± 20 µmol h^{-1} g^{-1}. NPs stabilized with SDS produced insufficient H_2 under 780 nm illumination for detection by gas chromatography. Samples of both TEBS- and SDS-stabilized Y6 NPs at the concentration used for H_2 evolution showed an absorbance above 1 in a 1-cm path length cuvette. The path length was increased to 2.3 cm within the liquid batch reactor, which further increased the absorbance. Due to this high light absorbance, both samples absorbed the majority of incident light.

Therefore, the EQE can be treated as an AQY.[29]

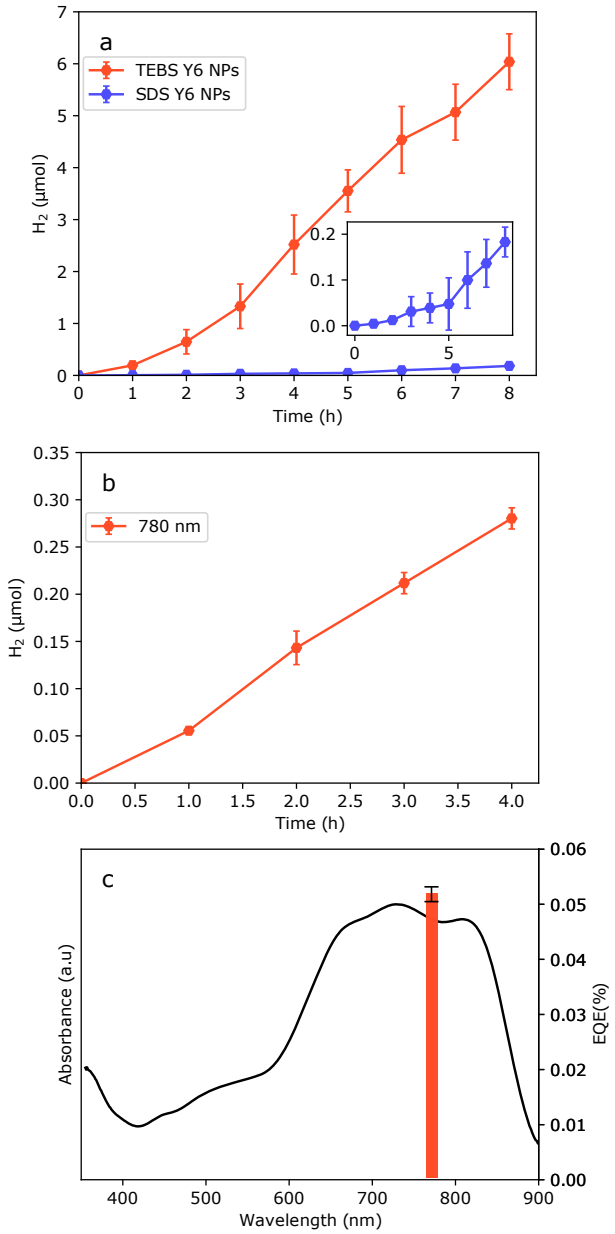

Figure 3: (a) Average H_2 evolution by Y6 NPs (0.225 mg) stabilized by SDS or TEBS under broadband illumination by 300 W Xe arc lamp (100 mW/cm^2) with ascorbic acid (0.2 M) as sacrificial electron donor and Pt co-catalyst (2% by mass). (b) H_2 evolution by TEBS-stabilized Y6 NPs under 780 nm illumination at intensity of 6.1 mW/cm^2; SDS-stabilized NPs produced no measurable H_2 under same conditions. (c) EQE of 0.054 $\pm$ 0.001 % for TEBS-stabilized Y6 at 780 nm, overlaid on the absorption spectrum of the NPs.

The rate of H_2 evolution and EQE exhibited by the TEBS-stabilized Y6 NPs is significantly lower than that of organic donor:NFA systems.[11,12] However, this decrease in performance for a single-component system is expected due to the loss of the bulk heterojunction structure, which provides a driving force for the separation of electrons and holes. The photocatalytic performance of Y6 NPs is more appropriately compared to the performance of single-component donor–acceptor co-polymer NPs. Contrasting the TEBS-stabilized Y6 NPs to donor–acceptor co-polymers with similar weight loading of Pt co-catalyst, Y6 exhibits a relatively low EQE but a rate of H_2 evolution higher than most.[7,10,34] This low EQE is likely due to the single-component nature of the NPs, in which there is a lower driving force for charge separation when compared to a donor:acceptor heterojunction. In Y6 films, most excited states are lost within ∼100 ps of excitation,,[24,27,35] indicating that the formation and persistence of free charges may be limited by exciton–exciton and charge recombination in the NP bulk. Y6 NPs have similarly short excited-state lifetimes, which are further discussed later in this article. However, despite the low EQE, Y6 NPs maintain a high rate of H_2 evolution per mass due to the strong and broad absorption of the NPs across the visible spectrum and particularly towards the near-infrared.

Figure 3 shows that the difference in H_2 evolution displayed by Y6 when stabilized by SDS or TEBS is significant. To understand the reason for such a significant difference in H_2 evolution between Y6 NPs stabilized by TEBS and SDS, we considered how Y6 NPs are able to evolve H_2. Studies of Y6, both on its own and in donor:Y6 blends, have suggested that the unique packing of the material allows Y6 excitons to partially[24] or fully[26,27] separate into free charges within Y6 domains, as well as at donor–Y6 interfacial sites. During photocatalysis, the generation of separated charges should allow the material to form surface deposits of Pt, through reduction of Pt cations by free electrons at the surface of the NP. The presence and quantity of Pt deposits is a large factor in photocatalytic performance. Each Pt deposit provides a surface site which is stable in a lower oxidation state, and promotes the physical separation of free electrons from holes, which reduces charge recombination.[36]

As the Pt co-catalyst is loaded through photodeposition, we can indirectly observe the rate of Pt deposition, as the rate of H_2 evolution exhibits a more exponential dependence on time while Pt is depositing, transitioning to a linear dependence once deposition is complete. Figure 3 shows that H_2 evolution by Y6 NPs stabilized by TEBS reaches the linear regime after ∼3 hours, while SDS-stabilized NPs achieve linearity after ∼5 hours. The additional time required to complete Pt photodeposition could be an indication of charge trapping at the NP surface in the SDS-stabilized NPs, or other surface effects lowering the ability of charges to facilitate reduction of Pt cations. To clarify any differences in Pt deposition between NPs formed with SDS or TEBS, the NPs were imaged by TEM.

Platinization of Y6 Nanoparticles

As discussed above, effective deposition of the Pt co-catalyst on the NP surface is critical for photocatalytic performance.[37] Pt deposits should be small to give a high surface-area-to-volume ratio, and distributed across the NP surface. If the NP has multiple components, then the Pt deposits should be located on the component that carries the free electron following exciton separation. Photocatalytic H_2 evolution is known to follow a volcano-type trend as the Pt loading is increased, with evolution rates initially increasing as charge recombination is suppressed, then decreasing as excessive Pt on the surface shields the NP from incident light absorption.[36] Pt photodeposition occurs through the reduction of Pt cations at the NP surface by donation of electrons from the semiconductor NP.[37] Hence, Pt deposition can be influenced by both the photophysics and the morphology of the NP.

We used TEM to image the NPs as prepared and after an 8 h photocatalysis experiment with 2 % Pt loading in the presence of sacrificial electron donor ascorbic acid (Figure 4). Due to the high electron density of Pt deposits compared to the Y6 NPs, the Pt deposits appear as small dark features on the surface and edges of the NPs. When the NPs are stabilized with TEBS, after photocatalysis the NPs are clearly covered in a disperse layer of small Pt deposits which appear to be distributed randomly across the NP surface (Figure

4c). However, when SDS is used, the density of Pt deposits is greatly reduced, with only a few Pt deposits found on each NP (Figure 4d). Poor Pt deposition inhibits the evolution of H_2 by the SDS-stabilized NPs, as shown in Figure 3a. This poor deposition may be due to the difference in the two surfactants, for example if SDS packs on the surface of the NP in such as way that it hinders the ability of Pt cations to reach the surface for deposition. To investigate the packing of the surfactants on the NP surface, we used zeta potential measurements to compare the surface charge density of the SDS- and TEBS-stabilized NPs.

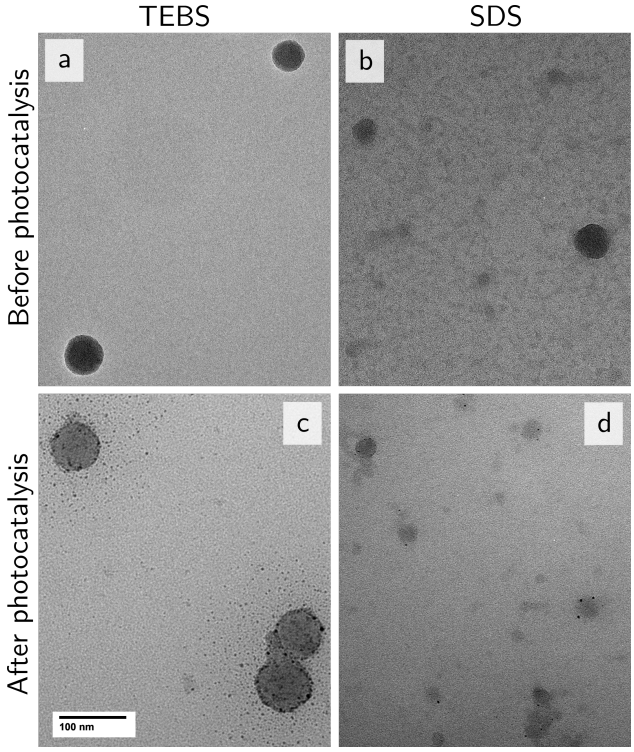

Figure 4: TEM images of Y6 NPs prepared with TEBS and SDS (a)–(b) before and (c)–(d) after photodeposition of Pt and photocatalysis. The scale is consistent between all four panels and the scale bar is given in the lower left corner of panel (c). Small nm-scale deposits of the Pt co-catalyst on the Y6 NP surface are visible as small dark spots in panels (c) and (d).

Zeta Potential

The low photocatalytic activity exhibited by SDS-stabilized Y6 NPs was further investigated by measuring the zeta potential (ζ) of both TEBS- and SDS-stabilized NPs. We found that

the zeta potential of SDS-stabilized Y6 NPs is $-57 \pm 4\,\mathrm{mV}$, 1.4 times larger in magnitude than the zeta potential of TEBS-stabilized Y6 NPs ($\zeta = -40 \pm 1\,\mathrm{mV}$). Under the assumption that the similar preparation methods for the two NPs suspensions result in similar solvent ionic strength, the difference in zeta potential is then equivalent to the difference in surface charge density of the Y6 NPs. For this difference in surface charge density to represent the difference in density of surfactant present over the surface of Y6 NPs, the extent of dissociation of the head groups of SDS and TEBS would have to be similar. Given that the zeta potential was measured in NP suspensions with a pH of 7, for this comparison to be accurate the pK_a of the acid equivalents of both surfactants would need to be similar, or sufficiently lower than 7 such that complete dissociation of both surfactants could be assumed. The pK_a of the acid equivalent of SDS, dodecyl sulfuric acid, is 5.82.[38] TEBS is a relatively novel surfactant, and hence the pK_a for its equivalent sulfonic acid is not known. However, sulfonic acids typically have lower pK_a values than their sulfuric acid counterparts. Therefore, the sulfonic acid equivalent of TEBS likely to have a pK_a value similar to other sulfonic acids ($-3 \lesssim \mathrm{p}K_\mathrm{a} \lesssim 3$[39]). Interestingly, during photocatalysis when ascorbic acid was present, highly acidic conditions were expected to result in a greater dissociation of TEBS than SDS due to the lower expected pK_a of the sulfonic acid. Hence, the use of TEBS potentially results in increased colloidal stability in acidic conditions.

As the equivalent acids for SDS and TEBS have pK_a values lower than the pH of the solvent, we assume both surfactants are essentially completely dissociated. Hence, the difference in surface charge density should be a good approximation of the difference in density of surfactant over the NP surface. The finding that Y6 NPs stabilized with SDS have a higher surface charge density than those stabilized with TEBS indicates a higher density of surfactant on the surface of the SDS-stabilized NPs. This result is consistent with the work by Cho et al.,[40] who found that polymer NPs stabilized with SDS had a high surface charge density and concluded that SDS likely formed a dense outer layer over the NP.[40] Our results follow the same trend, and lead to a similar conclusion: SDS likely forms a denser outer

layer over the NP than TEBS does, leading to an insulating effect over the surface of the SDS-stabilized NPs. To verify that this denser outer layer of SDS is the cause of decreased Pt deposition and hence photocatalytic activity, the photophysics of both NP suspensions were investigated using ultrafast TA spectroscopy.

Transient Absorption Spectroscopy

In the discussion above, we have shown that Y6 NPs stabilized with SDS have inferior H_2 evolution rates and poor Pt deposition compared to those stabilized with TEBS. Additionally, the surface charge density of Y6 NPs with the two surfactants indicates that the density of surfactant on the NP surface is higher when the NPs are stabilized with SDS. The increase in surface charge density when SDS is used suggests that the poor platinization and hence poor H_2 evolution rates may be due to SDS forming an insulating layer over the surface of the NPs and inhibiting Pt cations from reaching the surface and being reduced to Pt metal. However, there remains the possibility that in the SDS-stabilized NPs free charges are generated inefficiently, or are unable to effectively diffuse to the NP surface. To determine if there is any difference in the photophysics of the NP stabilized with SDS and TEBS, we used ultrafast TA spectroscopy to track the absorption of transient excited states on the picosecond–nanosecond timescale.

The photophysics of neat Y6 is known to be relatively complex. In Y6 films, the formation of long-lived triplets has been observed, which is characterized by a strong absorption around 1400 nm.[23,35,41] Triplets can be formed by both intersystem crossing and by singlet fission, where a highly excited singlet combines with a neighboring ground-state molecule to form two triplets.[42] Additionally, the initially excited Y6 singlet state has been observed to convert rapidly to a charge-transfer-like state, which is thought to be an intermediate to hole transfer in donor:Y6 blends.[24,43] Finally, in a number of dimer configurations the binding energy of Y6 excitons has been calculated to be very low (≤ 0.15 eV[26]), and free charge formation has been demonstrated in which in neat Y6 films.[26,27] There are few studies on whether

these species are also formed in Y6 NPs, which are likely to have morphological and hence photophysical differences compared to Y6 films.

We first assigned the TA data of Y6 NPs stabilized with TEBS (Figure 5). At <1 ps, the TA data (Figure 5a) have a strong ground-state bleach (GSB) signal from 620–880 nm, in the same region as the steady-state absorption of Y6 (Figure 2). However, there is a mismatch between the spectral shape of the GSB and steady-state absorption, where the steady-state absorption in this region is relatively broad and uniform, while the GSB is weaker than expected from 720 to 800 nm. This spectral feature is the result of a (positive) excited-state absorption (ESA) that overlaps with the negative GSB in this region. Additional ESA signals are observed in the <600 nm and >880 nm regions. Initially, Y6 is excited to the first singlet state by the 808 nm pump, and hence the spectral shape at <1 ps, which is characterized by an ESA peaking at ∼915 nm, is assigned to the TA of S_1. By normalizing the data to the GSB feature around 850 nm (Figure 5b), we show that the TA undergoes a continuous change in spectral shape over 4 ns. This shape change indicates that species other than the initially excited S_1 state are formed in these NPs and continue to evolve over 4 ns.

The shape change appears to occur in two stages. First, over the first 100 ps, the intensity of the GSB peak around 680 nm decreases relative to that of the 850 nm GSB peak, and at 780 nm the signal becomes less negative and approaches zero. The ESA at <600 nm is red-shifted, and the prominent singlet absorption at 915 nm is lost. Critically, the increase in the 780 nm signal appears in the same place as the known absorption of the Y6 anion in films.[22] Hence, we assign this shape change to the formation of free polarons in the Y6 NPs. The second stage of spectral change occurs on the nanosecond timescale, when the TA data has low amplitude and most excited species have returned to the ground state. This shape change is characterized primarily by a decrease in the signal at 780 nm and an increase in the >900 nm ESA, particularly towards 1000 nm. This decrease of the 780 nm feature along with the decay of the spectrum overall is assigned to the decay of free polarons, likely though charge recombination. The decay of free polarons leaves behind a small population

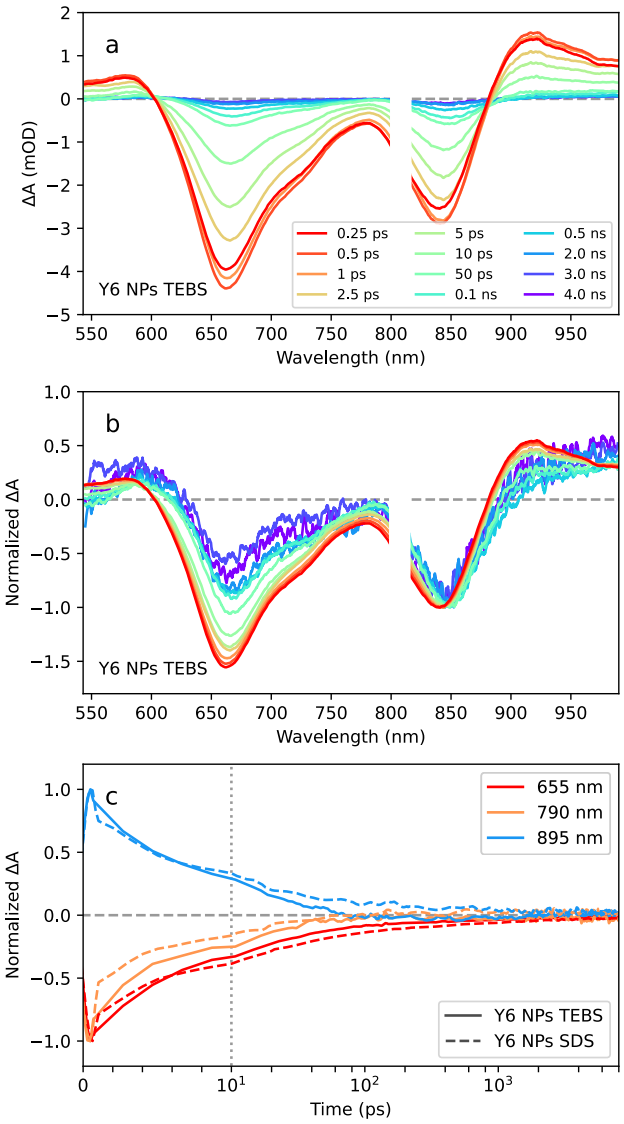

Figure 5: (a) TA data for Y6 NPs stabilized with TEBS excited at 808 nm with pump fluence of 11.2 µJ/cm^2. (b) Data in (a) normalized to the peak around 840 nm. Legend in (a) also applies to panel (b). (c) Kinetics of TA data at 655 nm, 790 nm, and 895 nm for Y6 NPs stabilized with TEBS and SDS at 11.2 µJ/cm^2 pump fluence. Dotted line indicates the transition from linear to logarithmic scaling on the time axis.

of a residual species, which we assign to triplets, which may be formed through intersystem crossing, singlet fission, or non-geminate charge recombination.[23,27,35,41] Under excitation at 800 nm, triplet formation in Y6 has been reported to occur through singlet–singlet annihilation, forming a highly-excited singlet state which subsequently undergoes singlet fission by interacting with a ground-state molecular to form two triplets.[35] Alternatively, Price et al. attributed the formation of triplets to non-geminate charge recombination.[27] Triplet formation by singlet fission or charge recombination is feasible at this power as the TA kinetics remain power-dependent (Figure S7), indicating that bi-molecular annihilation processes are present.

Figure 5c shows the evolution of the TA data for Y6 NPs stabilized with TEBS at selected wavelengths over time. Due to the significant spectral overlap between the absorption of various excited-state species in this system and the GSB, finding wavelengths that represents the kinetics of single species is challenging. Here, we have used the GSB signal at 655 nm to approximate the decay of all excited-state species in the system, as this signal appears to have the lowest overlap with the ESA from 680–800 nm. This signal decays rapidly, with most excited states lost within 100 fs of excitation. To represent the decay of the initially excited singlet, we have used the ESA at 895 nm, as this wavelength contains the minimal amount of interference from the ESAs assigned to polarons and triplets at >900 nm. This singlet signal also decays rapidly, but it decays somewhat faster than the GSB signal, indicating that while most singlet states decay rapidly to the ground state, a small population of singlets is converted to triplets and free polarons. Finally, we have used the known Y6 anion absorption at 790 nm to represent the formation of free polarons. This signal has a strong contribution from the overlapping GSB in this region and hence also decays rapidly. However, by comparing the kinetics at 790 nm to those at 655 nm, we find that the 790 nm signal decays faster than the GSB at 655 nm. This accelerated decay is due to the increasingly positive component of the signal corresponding to the formation of Y6 anions. The lifetime of the free polarons observed in these Y6 NPs is on the sub-nanosecond scale. This lifetime

is rather short for free polarons; in PM6:Y6 blend NPs, free polarons are known to live for up to 50 µs.[12] However, this short lifetime is expected as these NPs are single-component systems, and they lack the bulk heterojunction structure which helps to suppress electron–hole recombination by separating holes and electrons into donor and acceptor domains, respectively.

It has been shown that TA spectroscopy of platinized organic semiconductor NPs in the presence and absence of ascorbic acid can be used to demonstrate transfer of electrons to Pt and quenching of the remaining holes by ascorbic acid.[12] We performed TA spectroscopy on TEBS-stabilized Y6 NPs platinized with and without ascorbic acid (Figure S10). We observed a slightly faster decay of the kinetics at 655 nm, 790 nm, and 895 nm at times <10 ps when the NPs are platinized compared to as-prepared NPs However, the spectral shapes of the platinized NPs at these times are similar to the as-prepared NPs, indicating that the presence of Pt has a minor impact on distribution of species in the system. Therefore, the transfer of electrons to Pt and quenching of holes by ascorbic acid must either occur on a longer timescale than the 8 ns available here, or result in a change in the TA data that is unresolvable at this noise level. The EQE of this system is <0.1 %, indicating that only a very small proportional of Y6 excitations result in transfer of an electron to Pt. This small change in excited-state populations may be within the noise of our TA data.

To determine the effect of the surfactant on the photophysics, we compared the TA data for Y6 NPs prepared with SDS and TEBS. At early times, the spectral shape of TA data for NPs stabilized with SDS (Figure S11) is similar to that of the NPs stabilized with TEBS, and over time similar spectral shape changes are present in the data for both surfactants. Hence, the choice of surfactant has a negligible influence on the excited-state species of Y6 NPs. Furthermore, the kinetics at the three wavelengths described above are shown in Figure 5c. In the SDS-stabilized NPs, the ground state and singlet excited state are slightly longer lived than in the TEBS-stabilized NPs, particularly at intermediate times (10 ps to 1 ns). Additionally, the polaron ESA at 790 nm is more pronounced, increasing faster than

the same signal in the TEBS-stabilized NPs and becoming positive from 100 ps. These observations appear to indicate that, in the SDS-stabilized NPs, free polaron formation is more favorable than in the TEBS-stabilized NPs. Although free polarons are present in the SDS-stabilized NPs, the poor platinization of these NPs severely limits electron transfer to Pt. As a consequence, the SDS-stabilized NPs exhibit low H_2 evolution rates. In contrast, the effective platinization of the TEBS-stabilized NPs promotes efficient electron transfer from Y6 to Pt and results in higher H_2 evolution rates.

Conclusions

Here, we show that Y6 NPs stabilized with the thiophene-containing surfactant TEBS are effective HEPs with a Pt co-catalyst under sacrificial conditions, with a H_2 evolution rate of $4200 \pm 400\,\mu mol\,h^{-1}\,g^{-1}$ under broadband illumination from 400 nm to 900 nm. In contrast, Y6 NPs stabilized with SDS exhibit a rate of H_2 evolution 21 times lower at $110 \pm 20\,\mu mol\,h^{-1}\,g^{-1}$. TEM imaging of Y6 NPs reveals a lower amount of Pt co-catalyst deposited over the NPs stabilized by SDS when contrasted to those stabilized by TEBS. Additionally, the zeta potential of NPs stabilized by both surfactants indicates that the SDS-stabilized NPs have a higher surface charge density than the TEBS-stabilized NPs. This higher surface charge density may be attributed to a higher density of surfactant over the NPs surface when SDS is used. Ultrafast TA data show that there is minimal difference between the photophysics of the Y6 NPs stabilized with SDS or TEBS. Hence, the use of SDS or TEBS has a minor effect on the generation of free charges in the Y6 NPs. Rather, the formation of a dense insulating layer of SDS on the NP surface prevents the deposition of the Pt co-catalyst and hence reduces the H_2 evolution rate. This work highlights the understudied influence that surfactants can have over the surface reactions in NP photocatalysts, and encourages the use of thiophene-containing surfactants such as TEBS, even in single-component systems. Additionally, the reasonably high H_2 evolution rate of the TEBS-stabilized Y6 NPs suggests the potential use of the Y-series electron acceptors as HEPs in Z-scheme photocatalysts.

Supporting Information Description

(1) Energy levels of Y6; (2) Full DLS size distributions; (3) TEM images of NPs platinized in the presence and absence of ascorbic acid; (4) Further experimental details and data for photocatalysis; and (5) further TA data including power-dependent kinetics, SDS-stabilized NPs, and platinized NPs.

Acknowledgements

J.M.d.l.P acknowledges support from an Australian Government Research Training Program (RTP) Stipend, a Playford Trust PhD Scholarship, a Constance Fraser Supplementary Scholarship, and a Forrest George and Sandra Lynne Young Supplementary Scholarship. This work was supported by research grants from the Australian Research Council (DP160103797, DP220102900, LE0989747, and LE200100051). The authors thank Dr. Patrick Tapping for discussions contributing to this work, and Dr. Ashley Slattery for experimental assistance with TEM.

References

(1) Rogelj, J.; Schaeffer, M.; Meinshausen, M.; Knutti, R.; Alcamo, J.; Riahi, K.; Hare, W. Zero Emission Targets as Long-Term Global Goals for Climate Protection. *Environ. Res. Lett.* **2015**, *10*, 105007.

(2) Rogelj, J.; Den Elzen, M.; Höhne, N.; Fransen, T.; Fekete, H.; Winkler, H.; Schaeffer, R.; Sha, F.; Riahi, K.; Meinshausen, M. Paris Agreement Climate Proposals Need a Boost to Keep Warming Well Below 2ÂřC. *Nature* **2016**, *534*, 631–639.

(3) van Renssen, S. The Hydrogen Solution? *Nat. Clim. Change* **2020**, *10*, 799–801.

(4) Chen, S.; Takata, T.; Domen, K. Particulate Photocatalysts for Overall Water Splitting. *Nat. Rev. Mater.* **2017**, *2*, 17050.

(5) Sayama, K.; Miseki, Y. Research and Development of Solar Hydrogen Production: Toward the Realization of Ingenious Photocatalysis-Electrolysis Hybrid System. *Synthesiology* **2014**, *7*, 81–92.

(6) Nishiyama, H.; Yamada, T.; Nakabayashi, M.; Maehara, Y.; Yamaguchi, M.; Kuromiya, Y.; Nagatsuma, Y.; Tokudome, H.; Akiyama, S.; Watanabe, T. et al. Photocatalytic Solar Hydrogen Production from Water on a 100-m^2 Scale. *Nature* **2021**, *598*, 304–307.

(7) Wang, Y.; Vogel, A.; Sachs, M.; Sprick, R. S.; Wilbraham, L.; Moniz, S. J. A.; Godin, R.; Zwijnenburg, M. A.; Durrant, J. R.; Cooper, A. I. et al. Current Understanding and Challenges of Solar-Driven Hydrogen Generation using Polymeric Photocatalysts. *Nat. Energy* **2019**, *4*, 746–760.

(8) Hisatomi, T. Introductory Lecture: Sunlight-Driven Water Splitting and Carbon Dioxide Reduction by Heterogeneous Semiconductor Systems as Key Processes in Artificial Photosynthesis. *Faraday Discuss.* **2017**, *198*, 11–35.

(9) Seo, J.; Nishiyama, H.; Yamada, T.; Domen, K. Visible-Light-Responsive Photoanodes for Highly Active, Stable Water Oxidation. *Angew. Chem. Int. Ed.* **2018**, *57*, 8396–8415.

(10) Kosco, J.; Moruzzi, F.; Willner, B.; McCulloch, I. Photocatalysts Based on Organic Semiconductors with Tunable Energy Levels for Solar Fuel Applications. *Adv. Energy Mater.* **2020**, *10*, 2001935.

(11) Kosco, J.; Bidwell, M.; Cha, H.; Martin, T.; Howells, C. T.; Sachs, M.; Anjum, D. H.; Gonzalez Lopez, S.; Zou, L.; Wadsworth, A. et al. Enhanced Photocatalytic Hydrogen Evolution from Organic Semiconductor Heterojunction Nanoparticles. *Nat. Mater.* **2020**, *19*, 559–565.

(12) Kosco, J.; Gonzalez-Carrero, S.; Howells, C. T.; Fei, T.; Dong, Y.; Sougrat, R.; Harrison, G. T.; Firdaus, Y.; Sheelamanthula, R.; Purushothaman, B. et al. Generation of Long-Lived Charges in Organic Semiconductor Heterojunction Nanoparticles for Efficient Photocatalytic Hydrogen Evolution. *Nat. Energy* **2022**, *7*, 340–351.

(13) Ng, B.-J.; Putri, L. K.; Kong, X. Y.; Teh, Y. W.; Pasbakhsh, P.; Chai, S.-P. Z-Scheme Photocatalytic Systems for Solar Water Splitting. *Adv. Sci.* **2020**, *7*, 1903171.

(14) Zhang, H.; Tian, W.; Zhang, J.; Duan, X.; Liu, S.; Sun, H.; Wang, S. Carbon Nitride-Based Z-Scheme Photocatalysts for Non-Sacrificial Overall Water Splitting. *Mater. Today Energy* **2022**, *23*, 100915.

(15) Zhang, H.; Liu, J.; Jiang, L. Photocatalytic Hydrogen Evolution Based on Carbon Nitride and Organic Semiconductors. *Nanotechnology* **2022**, *33*, 322001.

(16) Pan, X.; Sharma, A.; Gedefaw, D.; Kroon, R.; de Zerio, A. D.; Holmes, N. P.; Kilcoyne, A. D.; Barr, M. G.; Fahy, A.; Marks, M. et al. Environmentally Friendly Preparation of Nanoparticles for Organic Photovoltaics. *Org. Electron.* **2018**, *59*, 432–440.

(17) Barr, M. G.; Chambon, S.; Fahy, A.; Jones, T. W.; Marcus, M. A.; Kilcoyne, A. D.; Dastoor, P. C.; Griffith, M. J.; Holmes, N. P. Nanomorphology of Eco-Friendly Colloidal Inks, Relating Non-Fullerene Acceptor Surface Energy to Structure Formation. *Mater. Chem. Front.* **2021**, *5*, 2218–2233.

(18) Subianto, S.; Balu, R.; de Campo, L.; Sokolova, A.; Dutta, N. K.; Choudhury, N. R. Sulfonated Thiophene Derivative Stabilized Aqueous Poly(3-hexylthiophene):Phenyl-C61-butyric Acid Methyl Ester Nanoparticle Dispersion for Organic Solar Cell Applications. *ACS Appl. Mater. Interfaces* **2018**, *10*, 44116–44125.

(19) Yan, C.; Barlow, S.; Wang, Z.; Yan, H.; Jen, A. K.-Y.; Marder, S. R.; Zhan, X. Non-Fullerene Acceptors for Organic Solar Cells. *Nat. Rev. Mater.* **2018**, *3*, 1–19.

(20) Cheng, P.; Li, G.; Zhan, X.; Yang, Y. Next-Generation Organic Photovoltaics Based on Non-Fullerene Acceptors. *Nat. Photonics* **2018**, *12*, 131–142.

(21) Li, X.; Lu, H.; Zhu, W. Recent Advances in Y6-Based Semiconductors: Performance in Solar Cells, Crystallography, and Electronic Structure. *ChemPlusChem* **2021**, *86*, 700–708.

(22) Natsuda, S.-i.; Saito, T.; Shirouchi, R.; Sakamoto, Y.; Takeyama, T.; Tamai, Y.; Ohkita, H. Cascaded Energy Landscape as a Key Driver for Slow yet Efficient Charge Separation with Small Energy Offset in Organic Solar Cells. *Energy Enviro. Sci.* **2022**, *15*, 1545–1555.

(23) Liang, S.; Li, S.; Zhang, Y.; Li, T.; Zhou, H.; Jin, F.; Sheng, C.; Ni, G.; Yuan, J.; Ma, W. et al. Efficient Hole Transfer via Delocalized Excited State in Small Molecular Acceptor: A Comparative Study on Photodynamics of PM6:Y6 and PM6:ITIC Organic Photovoltaic Blends. *Adv. Funct. Mater.* **2021**, *31*, 2102764.

(24) Wang, R.; Zhang, C.; Li, Q.; Zhang, Z.; Wang, X.; Xiao, M. Charge Separation from

an Intra-Moiety Intermediate State in the High-Performance PM6:Y6 Organic Photovoltaic Blend. *J. Am. Chem. Soc.* **2020**, *142*, 12751–12759.

(25) Kupgan, G.; Chen, X.; Brédas, J. Molecular Packing of Non-Fullerene Acceptors for Organic Solar Cells: Distinctive Local Morphology in Y6 vs. ITIC Derivatives. *Mater. Today Adv.* **2021**, *11*, 100154.

(26) Zhu, L.; Zhang, J.; Guo, Y.; Yang, C.; Yi, Y.; Wei, Z. Small Exciton Binding Energies Enabling Direct Charge Photogeneration Towards Low-Driving-Force Organic Solar Cells. *Angew. Chem. Int. Ed.* **2021**, *133*, 15476–15481.

(27) Price, M. B.; Hume, P. A.; Ilina, A.; Wagner, I.; Tamming, R. R.; Thorn, K. E.; Jiao, W.; Goldingay, A.; Conaghan, P. J.; Lakhwani, G. et al. Free Charge Photogeneration in a Single Component High Photovoltaic Efficiency Organic Semiconductor. *Nat. Commun.* **2022**, *13*, 1–10.

(28) Perdigón-Toro, L.; Zhang, H.; Markina, A.; Yuan, J.; Hosseini, S. M.; Wolff, C. M.; Zuo, G.; Stolterfoht, M.; Zou, Y.; Gao, F. et al. Barrierless Free Charge Generation in the High-Performance PM6:Y6 Bulk Heterojunction Non-Fullerene Solar Cell. *Adv. Mater.* **2020**, *32*, 1906763.

(29) Wang, Z.; Hisatomi, T.; Li, R.; Sayama, K.; Liu, G.; Domen, K.; Li, C.; Wang, L. Efficiency Accreditation and Testing Protocols for Particulate Photocatalysts toward Solar Fuel Production. *Joule* **2021**, *5*, 344–359.

(30) Savitzky, A.; Golay, M. J. Smoothing and Differentiation of Data by Simplified Least Squares Procedures. *Anal. Chem.* **1964**, *36*, 1627–1639.

(31) Zou, X.; Wen, G.; Hu, R.; Dong, G.; Zhang, C.; Zhang, W.; Huang, H.; Dang, W. An Insight into the Excitation States of Small Molecular Semiconductor Y6. *Molecules* **2020**, *25*, 4118.

(32) Wen, G.; Hu, R.; Su, X.; Chen, Z.; Zhang, C.; Peng, J.; Zou, X.; He, X.; Dong, G.; Zhang, W. Excited-State Properties of Y-Series Small Molecule Semiconductors. *Dyes Pigm.* **2021**, *192*, 109431.

(33) Lu, B.; Zhang, Z.; Jin, D.; Yuan, X.; Wang, J.; Ding, Y.; Wang, Y.; Yao, Y. A–DA'D–A Fused-Ring Small Molecule-Based Nanoparticles for Combined Photothermal and Photodynamic Therapy of Cancer. *ChemComm* **2021**, *57*, 12020–12023.

(34) Sprick, R. S.; Aitchison, C. M.; Berardo, E.; Turcani, L.; Wilbraham, L.; Alston, B. M.; Jelfs, K. E.; Zwijnenburg, M. A.; Cooper, A. I. Maximising the Hydrogen Evolution Activity in Organic Photocatalysts by Co-Polymerisation. *J. Mater. Chem. A* **2018**, *6*, 11994–12003.

(35) Natsuda, S.-i.; Sakamoto, Y.; Takeyama, T.; Shirouchi, R.; Saito, T.; Tamai, Y.; Ohkita, H. Singlet and Triplet Excited-State Dynamics of a Nonfullerene Electron Acceptor Y6. *J. Phys. Chem. C* **2021**, *125*, 20806–20813.

(36) Wang, Q.; Domen, K. Particulate Photocatalysts for Light-Driven Water Splitting: Mechanisms, Challenges, and Design Strategies. *Chem. Rev.* **2020**, *120*, 919–985.

(37) Wenderich, K.; Mul, G. Methods, Mechanism, and Applications of Photodeposition in Photocatalysis: A Review. *Chem. Rev.* **2016**, *116*, 14587–14619.

(38) Chirkst, D. E.; Lobacheva, O. L.; Berlinskii, I. V.; Sulimova, M. A. Recovery and Separation of Ce^{3+} and Y^{3+} Ions from Aqueous Solutions by Ion Flotation. *Russ. J. Appl. Chem.* **2009**, *82*, 1370–1374.

(39) Massoumi, B.; Aghili, H.; Entezami, A. Investigation of Electrochemical Copolymerization of 1-Naphthylamineaniline in the Presence of Various Organic Sulfonic Acids. *J. Chin. Chem. Soc.* **2009**, *56*, 741–747.

(40) Cho, J.; Cheon, K. H.; Ahn, H.; Park, K. H.; Kwon, S.-K.; Kim, Y.-H.; Chung, D. S. High Charge-Carrier Mobility of 2.5 $cm^{-2} V^{-1} s^{-1}$ from a Water-Borne Colloid of a Polymeric Semiconductor via Smart Surfactant Engineering. *Adv. Mater.* **2015**, *27*, 5587–5592.

(41) Gillett, A. J.; Privitera, A.; Dilmurat, R.; Karki, A.; Qian, D.; Pershin, A.; Londi, G.; Myers, W. K.; Lee, J.; Yuan, J. et al. The Role of Charge Recombination to Triplet Excitons in Organic Solar Cells. *Nature* **2021**, *597*, 666–671.

(42) Smith, M. B.; Michl, J. Recent Advances in Singlet Fission. *Ann. Rev. Phys. Chem.* **2013**, *64*, 361–386.

(43) Jasiūnas, R.; Zhang, H.; Devižis, A.; Franckevičius, M.; Gao, F.; Gulbinas, V. Thermally Activated Reverse Electron Transfer Limits Carrier Generation Efficiency in PM6:Y6 Non-Fullerene Organic Solar Cells. *Sol. RRL* **2022**, 2100963.

TOC Graphic

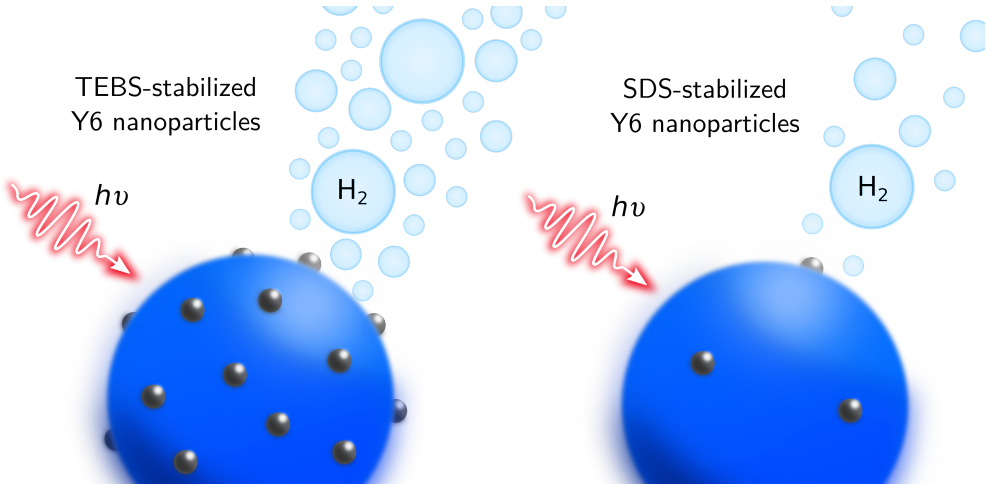
TEBS-stabilized
Y6 nanoparticles
hυ
H2
SDS-stabilized
Y6 nanoparticles
hυ
H2